Low-temperature-applicable polymer-stabilized blue-phase liquid crystal and its Kerr effect

Zhi-Gang Zheng (SID Member)
Hai-Feng Wang
Ge Zhu
Xiao-Wen Lin
Jia-Nan Li
Wei Hu (SID Member)
Hong-Qing Cui
Dong Shen
Yan-Qing Lu

Abstract — A type of polymer-stabilized blue-phase liquid crystal, which can be used in a low-temperature environment, is proposed. The blue-phase range after polymerization was widened to more than 73°C, and the blue-phase texture is very stable even at a temperature as low as –35°C. The electro-optical performances dependence on polymer concentration was investigated. The results indicate that the saturation voltage increases and the hysteresis enhances as the polymer concentration increases. The rise and decay times could reach as low as 391 and 789 μsec, respectively. Such material also shows good electro-optical behavior at a temperature of –35°C. In addition, the Kerr constant was tested under a uniformly distributed electric field to be 2.195 nm/V^2 at room temperature and 2.077 nm/V^2 at –35°C. The Kerr constant tested under white-light illumination was 1.975 nm/V^2, which shows a small dispersion.

Keywords — *Polymer-stabilized blue-phase liquid crystal, blue-phase range, response time, hysteresis, Kerr effect.*

DOI # 10.1889/JSID20.6.1

1 Introduction

The blue phase is a special liquid-crystal phase which has been attracting more and more attention in recent years. For its double-twisted liquid-crystal arrangement and exotic amorphous fog-like structure (BP III) or the self-assembled three-dimensional cubic lattices (BP I and II), blue phase shows great promise in wide-viewing-angle, high-optical-efficiency, fast-response flat-panel displays[1–3] and other optical elements, such as tunable gratings,[4] lenses,[5,6] and viewing-angle controllers.[7] The intriguing arrangement, for one thing, makes the blue-phase presence optically isotropic so that the blue-phase liquid-crystal (BPLC) display is alignment free; the ordered micro cubic lattices of the blue phase makes a very good laser cavity, so it is possible to be applied in a micro-laser.[8,9]

However, its narrow temperature range, normally 1–5°C, limits its applications.[10] To overcome this problem, many efforts have been made in the past 10 years, such as polymer-stabilized blue-phase liquid crystal (PSBPLC), first proposed by Kikuchi *et al*;[11] some special liquid crystal structures with a wide blue-phase range, *e.g.*, the bimesogen with a higher flexoelastic ratio, proposed by Coles *et al.*[12]; and the binaphthyl molecule, synthesized by Yoshizawa *et al*.[13] Except for those, the wide blue-phase range stabilized by nanoparticles and bent-shaped molecules were also noticed.[14–18] In the above several techniques, PSBPLC is widely used in devices because of its better performance. The so-called PSBPLC is such a material that was a polymer network to reinforce the defect in the blue phase, thus stabilizing the cubic structure and widening the blue-phase range. Many works on PSBPLC devices have been carried out in the past 3 years. The detailed simulations and experiments on the optimization of the electrode shape and dimensions,[1–3,19,20] the electric-field distribution in IPS-driven-based BPLC devices,[21] and the hysteresis effect[22,23] have been reported. Meanwhile, many new display models based on PSBPLC have been proposed, such as the transflective[24–28] and the dye-doped reflective guest host.[29] Some works on the Kerr effect are also significant.[30–33]

In this paper, we propose a type of PSBPLC material which not only has a wide temperature range, but also is applicable in a rather-low-temperature environment. The Kerr constant and its dispersion of PSBPLC were tested under a uniformly distributed electric field. The performances of the material at –35°C were also tested to show its properties at low temperature. In the next section, we present material preparations and testing methods; the temperature range, electro-optical performances, and Kerr effect of our material are discussed in Sec. 3; the conclusions are given in the last section.

2 Material preparations and testing methods

The PSBPLC precursor is mixed with chiral nematic liquid-crystal (N*LC) host and acrylate-based monomers. The N*LC host is prepared by mixing the conventional NLC (Δn = 0.168) and the chiral dopant R811 (supported by Merck) with a weight ratio of 3:1. The NLC is homemade, which is mainly mixed by 4′-pentylbiphenyl-4-carbonitrile, 4′-terphenyl-4-carbonitrile, 1-ethoxy-4-[(4′-pentylphenyl)

Z-G. Zheng, H-F. Wang, and D. Shen are with East China University of Science and Technology, Department of Physics, No. 130 Melong Rd., Shanghai, 200237 China; telephone +86-13-6717-27805, e-mail: zgzheng@ecust.edu.cn
G. Zhu, X-W. Lin, J-N. Li, W. Hu, and Y-Q. Lu are with the College of Engineering and Applied Sciences and the National Laboratory of Solid State Microstructures, Nanjing University, Nanjing, P.R. China.
H-Q. Cui is with the LCD R&D Center, Infovision Optoelectronics Corp., Kunshan, P.R. China.
© Copyright 2012 Society for Information Display 1071-0922/12/2006-01$1.00.

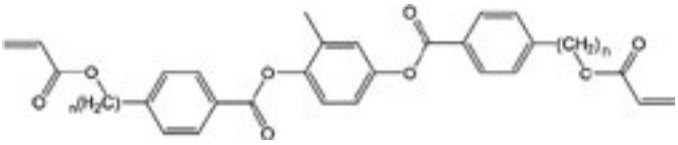

FIGURE 1 — Chemical structure of $PTPTP_n$, $PTPTP_3$ (n = 3), and $PTPTP_6$ (n = 6).

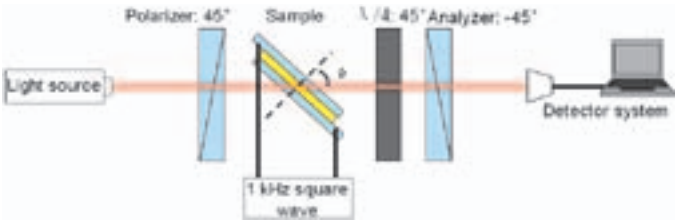

FIGURE 2 — Optical setup for phase-retardation testing.

ethynyl] benzene and 4′-pentylphenyl-4-ethoxybenzoate, with a weight ratio of 10:1:1:8. In addition, many other commercial NLCs can also be acceptable, such as the TEB series (supported by Slichem Co., Ltd.) or the XH series (supported by Xianhua Chemical Co., Ltd.). The monomers contain two components: one is the common 2-ethylhexyl acrylate (2-EHA) and the other is called $PTPTP_n$ (synthesized by our laboratory), which is mixed by $PTPTP_3$ and $PTPTP_6$ with a weight ratio of 1:1; their chemical structure is shown in Fig.1. The weight ratio between 2-EHA and $PTPTP_n$ is 1:2. All monomers have very good solubility with the N*LC host. To promote the polymerization of monomers under the UV exposure, a small amount of photoinitiators, Irgacure 184 (supported by Ciba), are also added to the mixture. The mixture is stirred at the clearing point for about 30 minutes and injected into an IPS cell by capillary action. The cell was statically placed in a dark box for several minutes to avoid flowing orientation, and then irradiated by the UV source for 360 sec. Thus, the PSBPLC sample is prepared. The irradiation intensity is 8.31 mW/cm^2.

The temperature range of the PSBPLC sample was tested by a precisely controlled hot stage, with a cooling or heating rate of 0.5°C/min. The voltage–transmittance (VT) curve was measured by placing the IPS cell between two crossed polarizers. The electrode direction of the cell is oriented at +/–45° to the polarizer's transmittance axis to reach maximum transmittance. The testing wavelength is 633 nm. The cell is driven by a square-wave signal with a frequency of 1 kHz. The response time was tested by applying a saturation voltage on the cell. The rise time is defined as the time for the transmittance to changes from 10% to 90% of the maximum transmittance, and the decay time is the time that the transmittance changes from 90% to 10% of the maximum transmittance.

The Kerr constant of the material is also a key parameter to evaluate the electro-optical performance. The normal method to test the Kerr constant is always to use the IPS cell, which supplies non-uniform electric fields.[1–3,19–21] Therefore, the configuration of electrodes and cell gaps will affect the measurement. In order to eliminate the influence of the cell structure, we use a simpler cell with just two planar electrodes, producing a uniform vertical electric field. The cell is settled obliquely with an angle θ to the propagation direction (as shown in Fig. 2). The oblique angle of the sample is adjusted from 5° to 55°, with a step of 5°. The real incident angle into the LC layer should be modified according to Snell's law, taking advantage of the refractive effect on the interface between the substrate and material. The average refractive index of the material tested by Abbe refractometer is 1.569; thus, the calculated angle onto the LC layer is 3.18°, corresponding to 5° onto the substrate.

The phase retardation was tested through the optical setup shown in Fig. 2, according to the well-known Senarmont method.[31] The sample was placed between the crossed polarizer and analyzer, and a quarter-wave plate was inserted before the analyzer with its fast axis parallel to the transmittance axis of the polarizer so that the transmittance reaches a minimum at the voltage-off state. When a field-induced phase retardation occurs, the transmittance increases. By rotating the analyzer to reach the minimal transmittance again, the phase retardation value could be calculated by the rotation angle.

3 Results and discussions

Five precursors with monomer concentration of 3, 5, 7, 9, and 12 wt.% were prepared. Their phase transitions were tested before UV exposure. The blue-phase width does not exceed 8°C, and it narrows as the monomer concentration increases. Furthermore, the phase-transition temperature of BP to the isotropic state ($T_{BP\text{-}Iso}$) decreases drastically, from 39.3°C with 3 wt.% monomers to 26.4°C with 12 wt.% monomers. The reason is related to the increase in amorphous 2-EHA in the mixture, which decreases the order parameter of LCs and narrows the LC phase range. The precursors are injected into the IPS cells (electrode width: 12 μm; electrode gap: 15 μm; cell gap: 5.2 μm) and irradiated for stabilization.

The temperature ranges after polymer stabilization are shown in Table 1. In addition, the blue-phase ranges of some materials mentioned in the Introduction are also listed to facilitate the comparison. The blue-phase range drastically extends as the monomer concentration increases. When the monomer is only 3 wt.% (PSBPLC1), the BP disappears at 24.3°C and the range is 9.7°C, only about 1–2°C larger than that before polymerization. As the monomer concentration increases to 5 wt.% (PSBPLC2), an evident decreasing of $T_{N^*\text{-}BP}$ to below –35°C and a slightly rise of $T_{BP\text{-}Iso}$ were observed. The BP range increases to more than 70.4°C, which is a great improvement compared to that of 3 wt.% monomers. As the monomer is keeps increasing (PSBPLC3–5), $T_{BP\text{-}Iso}$ increases further and $T_{N^*\text{-}BP}$ is also lower than –35°C, which is much lower than those reported previously as listed in the table. Limited by the testing range of our temperature controller, we could not give the exact value of $T_{N^*\text{-}BP}$ when it is lower than –35°C. The phase-

TABLE 1 — Phase-transition temperatures and blue-phase ranges for the PSBPLCs and some of the materials reported previously.

Sample (monomer concentration)	$T_{N^*\text{-}BP}$ /℃	$T_{BP\text{-}Iso}$ /℃	BP range/℃ ($\Delta T = T_{BP\text{-}Iso} - T_{N^*\text{-}BP}$)
PSBPLC1 (3 wt.%)	24.3	34.0	9.7
PSBPLC2 (5 wt.%)	<–35	35.4	>70.4
PSBPLC3 (7 wt.%)	<–35	38.2	>73.2
PSBPLC4 (9 wt.%)	<–35	38.2	>73.2
PSBPLC5 (12 wt.%)	<–35	38.2	>73.2
Kikuchi's PSBPLC[11]	–13	53	66
Bimesogen[12]	16	60	44
Binaphthyl[13]	43.3	72.2	~29
Nanoparticle stabilized[14]	28.6	33.6	5
Bent-shaped molecule stabilized[15]	53.4	82.5	~29

transition temperatures are tested during both cooling and heating, the reversibility between chiral nematic phase to blue phase and blue phase to isotropic seems good and no super-cooling of BP I is found in PSBPLC2–5. So it is believable that the BP texture can be stabilized when the monomer concentration is higher than 5 wt.%. The textures of PSBPLC2–5 are observed by using a polarized optical microscope (POM) with the crossed polarizers at room temperature. As shown in Fig. 3, the typical colorful platelets are presented in PSBPLC 2 and 3. The color is caused by the selective reflection of the BP domains. However, in PSBPLC4, the dimension of colorful domain is significantly smaller. As for PSBPLC5, the colorful domains are too small to be observed, leading to an almost dark field [Fig. 3(d)]. The difference of the domain size between the samples might be correlated to the change in polymer density in the samples. We can find in our experiments that the high polymer concentration leads to smaller BP domains.

A 1-kHz square-wave signal is applied on PSBPLC2–5, respectively. We found that PSBPLC2 is not stable under an electric field. When the voltage rises to 55 V, the blue-phase domains are destroyed and gradually transforms to the chiral nematic phase [Fig. 3(e)]. The chiral nematic phase can not recover to the blue phase even after the electric field is removed for about 12 hours. Such electric instability may be caused by two aspects: (1) the loose polymer network which could not suppress the collapse of the BP lattice under a high electric field; (2) the polymer-network distortion, which destroys the original double-twisted arrangement of LCs.[34] The BP textures in the other PSBPLCs are stable against applied voltages. VT curves for the three samples, PSBPLC3–5, were tested at room temperature. For the convenience of comparison, the transmittance of the sample is normalized to the peak maximum transmittance of its own. As shown in Fig. 4, VT curves of all samples present the same trend that the transmittance increases as the voltage rises up, and then reaches a saturation value. The result is a little different with that reported in some other publications, in which the transmittance reaches a peak value, and then decline gradually to saturation due to the small cell gap of the IPS cell; thus, the phase retardation of the entire cell is not enough to modulate one π. In addition, it is also evident that the drive voltage increases as the monomer concentration increases; and the hysteresis effect is more evident in the sample of the high polymer content, such as PSBPLC5. These results are mainly attributed to the stronger anchoring effect of the denser polymer network, which increases the rotation energy of LCs and restrains the recovery of LCs. To facilitate a comparison, we list the drive voltage at half-transmittance V_{50} and the hysteresis voltage ΔV_{50} of the samples in Table 2. Comparing PSBPLC3 with PSBPLC5, it is clear that the drive voltage rises about 60 V and the hysteresis

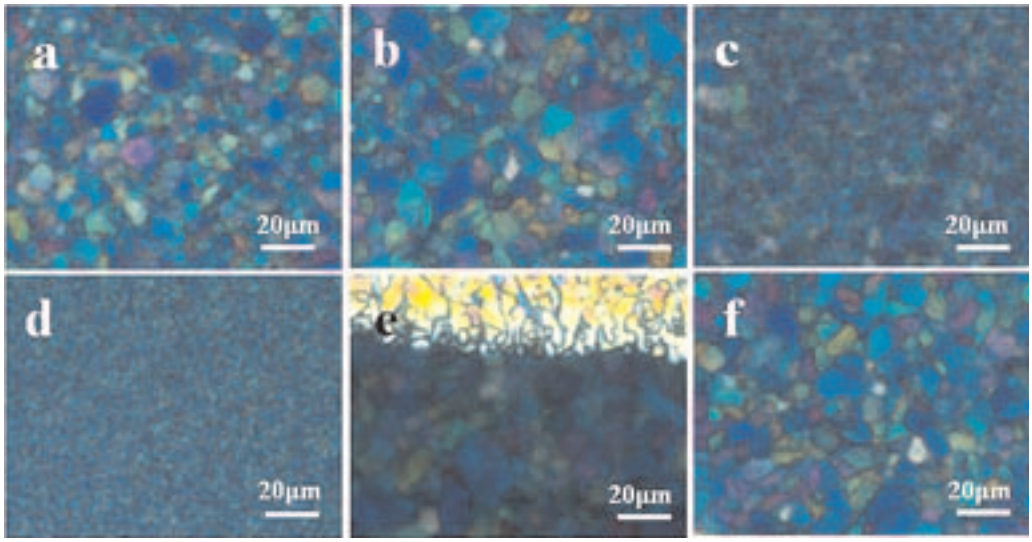

FIGURE 3 — BP textures observed through polarized optical microscope. (a) PSBPLC2, (b) PSBPLC3, (c) PSBPLC4, (d) PSBPLC5. (e) texture of PSBPLC2 after applying a 55-V voltage. (f) texture of PSBPLC3 at –35°C.

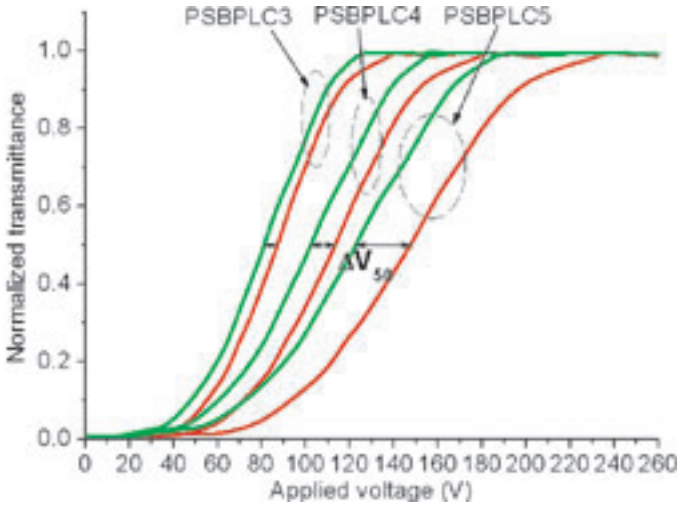

FIGURE 4 — VT curves of the PSBPLCs. The red curve stands for increasing the voltage gradually; the green curve stands for decreasing the voltage gradually. The hysteresis voltage at 50% transmittance is denoted as ΔV_{50} in the photograph.

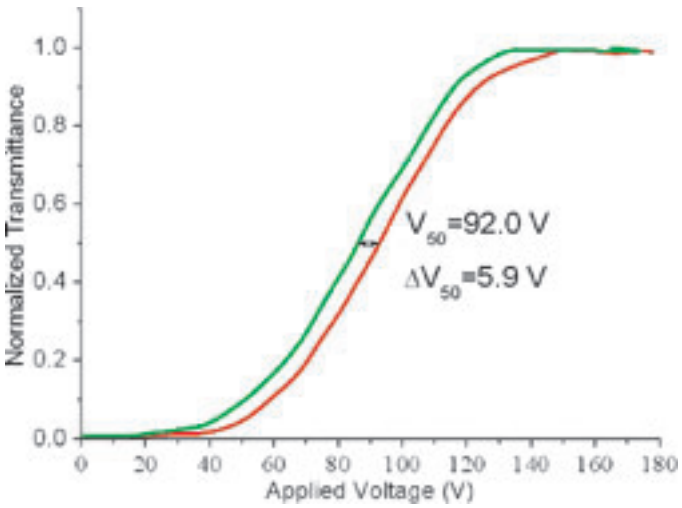

FIGURE 5 — VT curve of PSBPLC3 at –35°C.

voltage increases about 3.5 times. The response time of the samples were also tested and are given in Table 2. The decay time declines for the larger elastic constant in the sample with a denser polymer network. Besides, there is also a 20-μsec increase in rise time. We consider that the increase might be related to the larger anchoring energy to LCs in the high-polymer-content sample.

For the above results, 7 wt.% of monomer is considered as an optimal concentration. The PSBPLC3 was tested at a low temperature. The sample is slowly cooled to –35°C, and then held for 24 hours. The texture remains stable as observed by POM [as shown in Fig. 3(f)]. The sample is kept at –35°C, and its VT curve at low temperature is tested. As shown in Fig. 5, the voltage-modulated performance is very good. The trend of the curve is almost the same with that tested at room temperature (as shown in Fig. 4). The drive voltage and the hysteresis voltage are 92.0 and 5.9 V, respectively. Compared with the values tested at room temperature, the drive voltage presents a small increase, about 6.2%, and the hysteresis voltage also increases about 5.4%. The rise and decay times tested at this temperature are 400 and 805 μsec, respectively (listed in Table 2), about 2% larger than those at room temperature. The changes on the VT curve and response time may be caused by the increasing viscosity of LCs at low temperature. In a word, PSBPLC3 is applicable at a low temperature range with good performance, and such performance is very important for those LCDs that are used outdoors in the winter.

TABLE 2 — Drive voltage (V_{50}), hysteresis voltage (ΔV_{50}), rise time, and decay time of PSBPLC3–5. The data in the brackets were tested at –35°C.

Samples	V_{50}	ΔV_{50}	Rise time	Decay time
PSBPLC3	86.6 V	5.6 V	391 μsec (400 μsec)	789 μsec (805 μsec)
PSBPLC4	113.5 V	11.4 V	401 μsec	708 μsec
PSBPLC5	147.1 V	24.2 V	410 μsec	600 μsec

Next, the Kerr effect of PSBPLC3 was investigated under a uniformly distributed electric field. As mentioned in Sec. 2, we used a conventional LC cell with two ITO planar electrodes on the inner surface of the substrate to produce a uniform vertical electric field. Meanwhile, the Senarmont method was applied to test the phase retardation at a certain oblique angle θ (as shown in Fig. 2). Figure 6 shows the electric-field-dependent birefringence at some specific oblique angles. It is evident that the birefringence increases with the strengthening of the electric field. Moreover, the birefringence shows a trend that first increases rapidly at a low electric field, and then approaches saturation gradually in the strong electric field range, coincident with the extended Kerr effect. Moreover, it also can be found that the birefringence at the voltage-off state is not exactly 0, but a certain constant of about 0.6×10^{-3}. The small birefringence is not an occasional or experimental deviation, and we consider that it might be caused by the very small distortions of the BP lattice and the polymer network. Doping some high HTP chiral into the N*LC host suppresses the distortion, decreasing the dimensions of the BP domains or stabilizing the BP III texture may be the feasible way to solve this problem.[35,36]

Kerr constants corresponding to the certain oblique angles can be calculated through the electric-field-dependent birefringence curves. By considering the extended Kerr effect, the Kerr constant can be obtained by linearly fitting the experimental data at the weak-field region, and the slope of the straight line is the Kerr constant. Figure 7(a) gives the tested Kerr constants at some certain oblique angles. These data fit very well with the red straight line, and a fitted equation is obtained. The equation contains two terms: one is related to the oblique angle and the other is an angle-independent small constant, only 0.005 nm/V^2. We assume that the second term comes from the residual birefringence mentioned above. According to the fitted equation, the maximum of the Kerr constant is obtained when

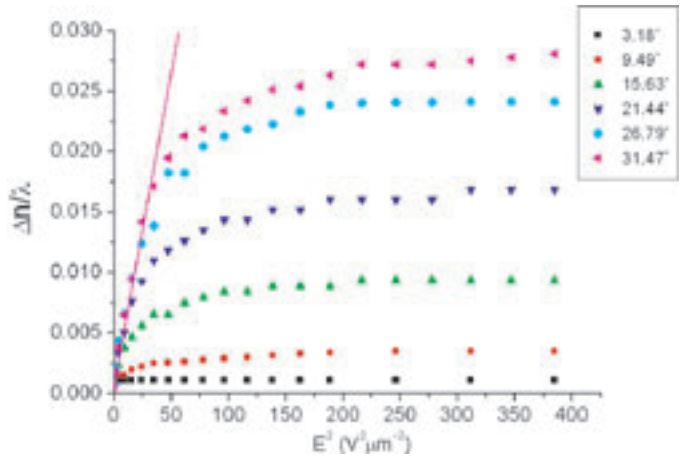

FIGURE 6 — Electric-field-dependent birefringence of PSBPLC3. The straight line is the linear fitting under a weak electric-field approximation when θ = 31.47°. The angles are calculated by Snell's law.

the oblique angle is 90°, which equals 2.195 nm/V^2. The Kerr constant under the weak-field approximation was studied in a previous work[30]; according to that, the equation of the oblique-angle-related Kerr constant can be expressed as

$$K_\theta = \frac{3\Delta n_{sat}}{\lambda E_s^2}\sin^2\theta + K_R \qquad (1)$$

in which Δn_{sat} is the saturated birefringence, E_s is the saturated electric field, and K_R is the Kerr constant caused by the residual birefringence. According to the results shown in Fig. 6, the saturation electric field can be obtained. By substituting E_s = 13.6 V/μm, K_R = 0.005 nm/V^2, K_{90} = 2.195 nm/V^2, and λ = 0.633 μm into Eq. (1), we can evaluate the saturation birefringence of PSBPLC3 to be about 0.0854. We can also analyze the dependence of the Kerr constant on the polymer concentration according to Eq. (1). By increasing the polymer, Δn_{sat} decreases because the polymer is isotropic; however, the E_s increases as tested and shown in Fig. 4, thus it can be believed that the Kerr constant decreases drastically. Besides, the Kerr constant of PSBPLC3 at –35°C was tested, and the oblique-angle-dependent Kerr constant is shown in Fig. 7(b). We only tested seven data points because the testing beam is blocked by the hot stage at a large oblique angle. However, these data also show good linearity and fit well with a straight line. The Kerr constant, 2.077 nm/V^2, obtained by the fitted equation

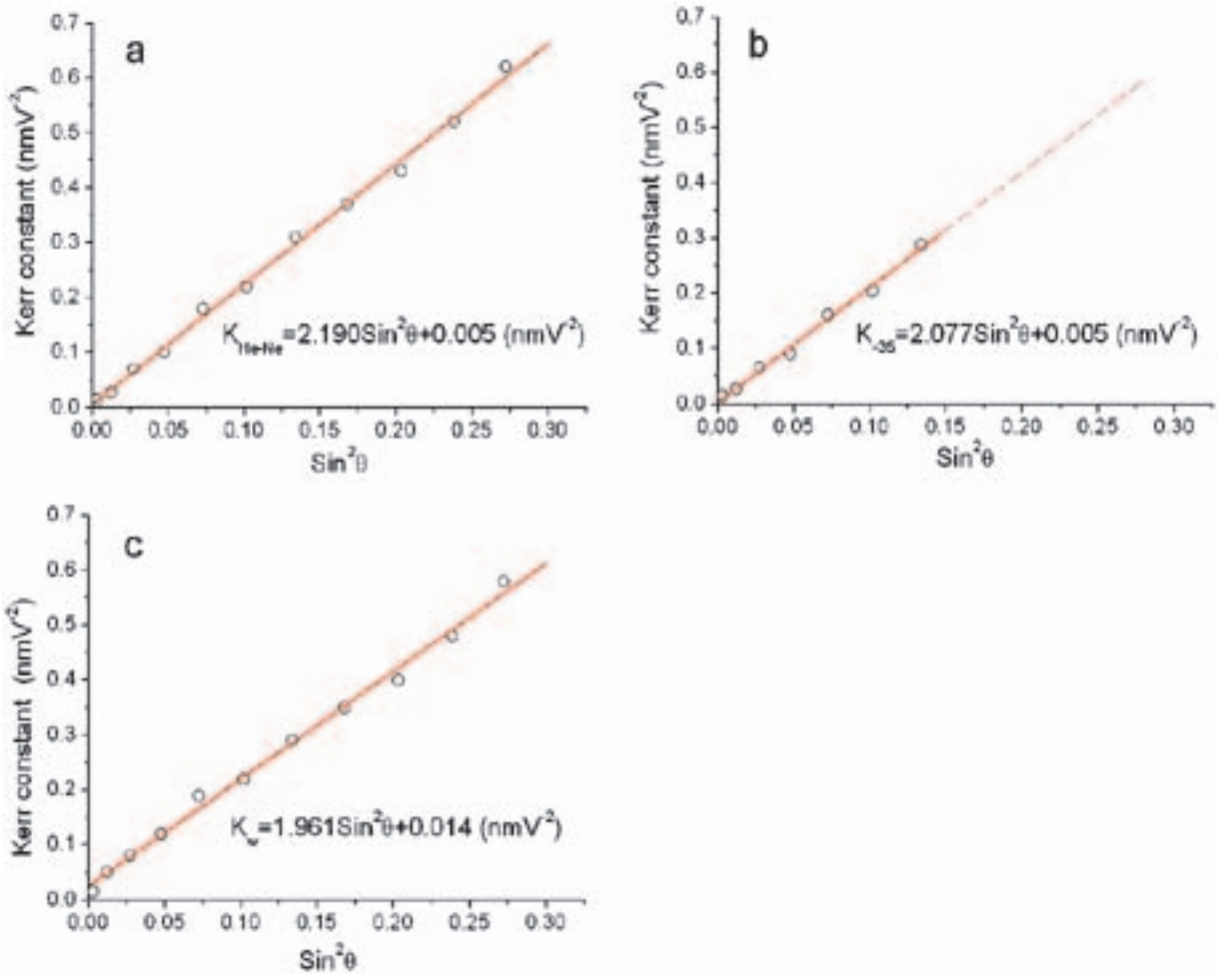

FIGURE 7 — The oblique-angle-dependent Kerr constant of PSBPLC3. Circles represent the experimental data; the red straight lines are fitted lines, and the fitted equations are given: (a) at room temperature (@ 633 nm); (b) at –35°V (@ 633 nm); (c) at room temperature (@ white light).

slightly decreases with increasing viscosity of the LCs for such a low temperature.

LCDs usually works under white-light illumination; the Kerr effect under the white light is very important. So, we change the He–Ne laser to a broadband white light source, and then test the Kerr constant of PSBPLC3 with the same method mentioned above. The oblique-angle-dependent Kerr constant are shown in Fig. 7(c). From the fitted equation, the Kerr constant under white-light illumination is about 1.975 nm/V^2, which is about 0.22 nm/V^2 smaller than that tested with a He–Ne laser. The difference can be interpreted as the dispersion of the Kerr constant.[37]

4 Conclusions

The PSBPLC material which works at low temperature was fabricated. The electro-optical performances of the material were evaluated from four aspects: the temperature range, drive voltage, hysteresis voltage, and the response time. From these evaluations, an optimal monomer concentration to fabricate PSBPLC was obtained. The VT curve and response time of the optimal material were tested at the room temperature and compared with those tested at –35°C. In addition, the Kerr constant at room temperature and –35°C were tested under a uniform electric field. From the results of the VT curve, the response time, and the Kerr constant, the low-temperature performance of the material is very good, and such a material is expected to be applied in low-temperature environments. The Kerr constant was also tested under white-light illumination, and the result shows a slight dispersion effect on our material.

Acknowledgments

This work was sponsored by the National Science Foundation of China (Grant No. 61108065), NSFJP program (Grant No. BK2010360), the Fundamental Research Funds for the Central Universities (Grant No. WM1014015), and supported by the China Postdoctoral Science Foundation (Grant No. 20110491370). The authors also offer their grateful thanks for the support from Infovision Optoelectronics Corporation.

References

1 Z. Ge *et al.*, "Electro-optics of polymer-stabilized blue phase liquid crystal displays," *Appl. Phys. Lett.* **94**, 101101 (2009).
2 L. Rao *et al.*, "Low voltage blue-phase liquid crystal displays," *Appl. Phys. Lett.* **95**, 231101 (2009).
3 M. Jiao *et al.*, "Low voltage and high transmittance blue-phase liquid crystal displays with corrugated electrodes," *Appl. Phys. Lett.* **96**, 011102 (2010).
4 J. Yan *et al.*, "High-efficiency and fast-response tunable phase grating using a blue phase liquid crystal," *Opt. Lett.* **36**, 1404–1406 (2011).
5 Y. H. Lin *et al.*, "Polarizer-free and fast response microlens arrays using polymer-stabilized blue phase liquid crystals," *Appl. Phys. Lett.* **96**, 113505 (2010).
6 Y. Li and S. T. Wu, "Polarization independent adaptive microlens with a blue-phase liquid crystal," *Opt. Express* **19**, 8045–8050 (2011).
7 L. W. Liu *et al.*, "A continuous-viewing-angle-controllable liquid-crystal display using a blue-phase liquid crystal," *J. Soc. Info. Display* **19**, 547–550 (2011).
8 W. Cao *et al.*, "Lasing in a three-dimensional photonic crystal of the liquid crystal blue phase II," *Nature Mater.* **1**, 111–113 (2002).
9 S. Yokoyama *et al.*, "Laser emission from a polymer-stabilized liquid-crystalline blue phase," *Adv. Mater.* **18**, 48–51 (2006).
10 Y. Hisakado *et al.*, "Large electro-optic Kerr effect in polymer-stabilized liquid-crystalline blue phases," *Adv. Mater.* **17**, 96–98 (2005).
11 H. Kikuchi *et al.*, "Polymer-stabilized liquid crystal blue phases," *Nature Mater.* **1**, 64–68 (2002).
12 H. J. Coles and M. N. Pivnenko, "Liquid crystal 'blue phase' with a wide temperature range," *Nature* **436**, 997–1000 (2005).
13 A. Yoshizawa *et al.*, "A binaphthyl derivative with a wide temperature range of a blue phase," *J. Mater. Chem.* **19**, 5759–5764 (2009).
14 H. Yoshida *et al.*, "Nanoparticle-stabilized cholesteric blue phases," *Appl. Phys. Express* **2**, 121501 (2009).
15 Z. Zheng *et al.*, "Wide blue phase range of chiral nematic liquid crystal doped with bent-shaped molecules," *New J. Phys.* **12**, 113018 (2010).
16 Z. Zheng *et al.*, "The liquid crystal blue phase induced by bent-shaped molecules with different terminal chain lengths," *New J. Phys.* **13**, 063037 (2011).
17 G. Zhu *et al.*, "Liquid crystal blue phase induced by bent-shaped molecules with allylic end groups," *Opt. Mater. Express* **1**, 1478–1483 (2011).
18 H. F. Wang *et al.*, "Blue phase liquid crystals induced by bent-shaped molecules based on 1,3,4-oxadiazole derivatives," *Liq. Cryst.* **39**, 99–103 (2011).
19 S. Yoon *et al.*, "Optimization of electrode structure to improve the electro-optic characteristics of liquid crystal display based Kerr effect," *Liq. Cryst.* **37**, 201–208 (2010).
20 L. Rao *et al.*, "Zigzag electrodes for suppressing the color shift of Kerr effect-based liquid crystal displays," *J. Display Technol.* **6**, 115–120 (2010).
21 Z. Ge *et al.*, "Modeling of blue phase liquid crystal displays," *J. Display Technol.* **5**, 250–256 (2009).
22 K. M. Chen *et al.*, "Hysteresis effects in blue-phase liquid crystals," *J. Display Technol.* **6**, 318–322 (2010).
23 L. Rao *et al.*, "Critical field for a hysteresis-free BPLC device," *J. Display Technol.* **7**, 627–629 (2011).
24 J. P. Cui *et al.*, "Transflective blue-phase liquid crystal display with corrugated electrode structure," *J. Soc. Info. Display* **19**, 709–712 (2011).
25 C. Song *et al.*, "Low voltage and high transmittance transflective display using polymer-stabilized blue-phase liquid crystal," *J. Display Technol.* **7**, 250–254 (2011).
26 F. Zhou *et al.*, "A single-cell-gap transflective display using a blue-phase liquid crystal," *J. Display Technol.* **7**, 170–173 (2011).
27 J. P. Cui *et al.*, "Transflective blue-phase liquid crystal display using an etched in-plane switching structure," *J. Display Technol.* **7**, 398–401 (2011).
28 D. Wu *et al.*, "Low voltage and high optical efficiency single-cell-gap transflective display using a blue-phase liquid crystal," *J. Display Technol.* **7**, 459–462 (2011).
29 Y. H. Lin *et al.*, "A reflective polarizer-free electro-optical switch using dye-doped polymer-stabilized blue phase liquid crystals," *Opt. Express* **19**, 2556–2561 (2011).
30 J. Yan *et al.*, "Extended Kerr effect of the polymer-stabilized blue-phase liquid crystals," *Appl. Phys. Lett.* **96**, 071105 (2010).
31 J. Yan *et al.*, "Direct measurement of electric-field-induced birefringence in a polymer-stabilized blue-phase liquid crystal composite," *Opt. Express* **18**, 11450–11455 (2010).
32 Y. Li *et al.*, "Dielectric dispersion on the Kerr constant of blue phase liquid crystals," *Appl. Phys. Lett.* **99**, 181126 (2011).
33 Y. H. Lin *et al.*, "Measuring electric-field-induced birefringence in polymer stabilized blue phase liquid crystal based on phase shift measurement," *J. Appl. Phys.* **109**, 104503 (2011).
34 J. Yan and S. T. Wu, "Effect of polymer concentration and composition on blue phase liquid crystals," *J. Display Technol.* **7**, 490–493 (2011).
35 C.-Y. Fan *et al.*, "Influence of polymerization temperature on hysteresis and residual birefringence of polymer stabilized blue phase LCs," *J. Display Technol.* **7**, 615–618 (2011).
36 A. Yoshizawa *et al.*, "Amorphous blue phase III exhibiting submillisecond response and hysteresis-free switching at room temperature," *Appl. Phys. Express* **4**, 101701 (2011).
37 M. Jiao *et al.*, "Dispersion relation on the Kerr constant of a polymer-stabilized optically isotropic liquid crystal," *Phys. Rev. E* **83**, 041706 (2011).

Zhi-gang Zheng received his Ph.D. degree from the Chinese Academy of Sciences in 2009. He then joined East China University of Science and Technology (ECUST). Currently, he is working in the Laboratory of Liquid Crystal Materials and Devices of ECUST. His research interest includes new optically isotropic liquid-crystal materials and devices, light-sensitive liquid-crystal materials and devices, liquid-crystal/polymer composites, bent-core materials, the molecular designing of liquid crystals, and liquid-crystal applications in THz fields. He has published more than 30 papers. He has been a SID member since 2009.

Wei Hu received his Ph.D. degree from Jilin University, Changchun, China, in 2009. He is currently a Lecturer at the College of Engineering and Applied Sciences and the National Laboratory of Solid State Microstructures, Nanjing University, Nanjing, China. His research is focused on liquid-crystal electro-optical materials and devices at present. He has published 18 peer-reviewed scientific papers, one book chapter, 12 conference contributions, and 11 patents and patent applications with his collaborators.